Structure of the D2 dopamine receptor bound to the atypical antipsychotic drug risperidone

Sheng Wang[1], Tao Che[1], Anat Levit[2], Brian K. Shoichet[2], Daniel Wacker[1] & Bryan L. Roth[1,3,4]

Dopamine is a neurotransmitter that has been implicated in processes as diverse as reward, addiction, control of coordinated movement, metabolism and hormonal secretion. Correspondingly, dysregulation of the dopaminergic system has been implicated in diseases such as schizophrenia, Parkinson's disease, depression, attention deficit hyperactivity disorder, and nausea and vomiting. The actions of dopamine are mediated by a family of five G-protein-coupled receptors[1]. The D2 dopamine receptor (DRD2) is the primary target for both typical[2] and atypical[3,4] antipsychotic drugs, and for drugs used to treat Parkinson's disease. Unfortunately, many drugs that target DRD2 cause serious and potentially life-threatening side effects due to promiscuous activities against related receptors[4,5]. Accordingly, a molecular understanding of the structure and function of DRD2 could provide a template for the design of safer and more effective medications. Here we report the crystal structure of DRD2 in complex with the widely prescribed atypical antipsychotic drug risperidone. The DRD2–risperidone structure reveals an unexpected mode of antipsychotic drug binding to dopamine receptors, and highlights structural determinants that are essential for the actions of risperidone and related drugs at DRD2.

DRD2 is essential for mediating the actions of antipsychotic drugs[2–4,6] and those of medications used to treat Parkinson's disease, hyperprolactinaemia, and nausea and vomiting, among many other disorders[1,7,8]. DRD2 has also been implicated in the actions of several drugs of abuse including amphetamines, cocaine and opioids[9]. Although DRD2 was cloned nearly 30 years ago[10–12] and has been subject to extensive pharmacological[13], mutagenesis[14] and molecular-modelling studies[15], we lack high resolution structures of DRD2 in complex with ligands, limiting our molecular understanding of its function. A 3.2 Å crystal structure of the related D3 dopamine receptor (DRD3)[16] and 1.95 Å and 2.2 Å structures of the D4 dopamine receptor (DRD4) have been reported[17]. The DRD3 and DRD4 ligand complexes—obtained with the substituted benzamides eticlopride and nemonapride, respectively—revealed distinctive extended binding sites[16,17]. Given the importance of DRD2-targeted drugs, and recent successes in using structures of G-protein-coupled receptors (GPCRs) to guide discovery of new chemical probes and therapeutic leads[18,19], the structure of DRD2 complexed with non-benzamide ligands will not only clarify the specificity determinants of the family, but will also expand our understanding of how different scaffolds interact with dopamine receptors. We anticipate that the ligand discovery enabled by DRD2 structures will therefore inform both basic and translational neuroscience[20].

We carried out structural studies using a human DRD2 construct, which included three thermostabilizing mutations (I122$^{3.40}$A, L375$^{6.37}$A and L379$^{6.41}$A; superscript refers to the Ballesteros–Weinstein numbering system for GPCRs[7]) and T4 lysozyme (T4L) fused into intracellular loop 3 (Extended Data Fig. 1a, b and Methods).

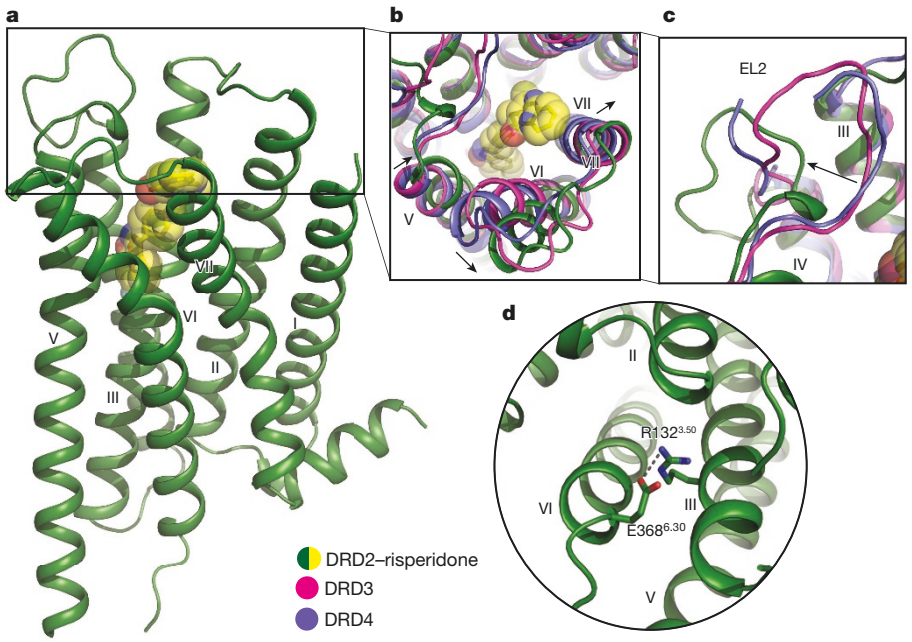

Figure 1 | Structural details of DRD2 and comparison with DRD3 and DRD4. Dopamine receptor structures are shown aligned to DRD2. Green, DRD2; magenta, DRD3 (PDB code: 3PBL); blue, DRD4 (PDB code: 5WIU). Risperidone (yellow) is shown in sphere representation. **a**, Overall structure of the DRD2–risperidone complex. **b**, **c**, Comparison of the view from the extracellular side. **d**, Cytoplasmic surface showing a salt-bridge interaction (grey dotted line) between R132$^{3.50}$ and E368$^{6.30}$.

[1]Department of Pharmacology, University of North Carolina at Chapel Hill, Chapel Hill, North Carolina 27599-7365, USA. [2]Department of Pharmaceutical Chemistry, University of California San Francisco, San Francisco, California 94158-2280, USA. [3]Division of Chemical Biology & Medicinal Chemistry, Eshelman School of Pharmacy, University of North Carolina at Chapel Hill, Chapel Hill, North Carolina 27599-7360, USA. [4]National Institute of Mental Health Psychoactive Drug Screening Program (NIMH PDSP), School of Medicine, University of North Carolina at Chapel Hill, Chapel Hill, North Carolina 27599-7365, USA.

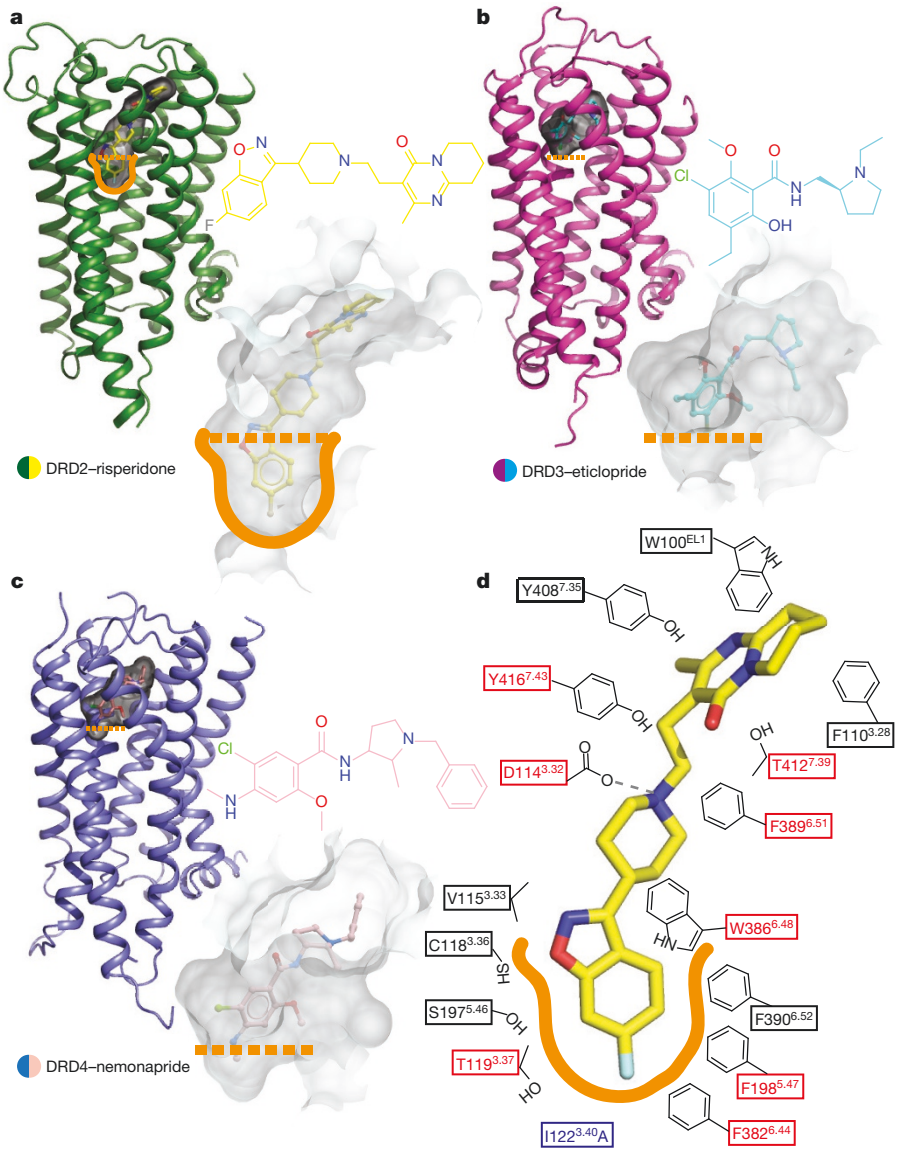

Figure 2 | Comparison of the ligand-binding pocket across the D2-like family receptors. **a**–**c**, Surface representations of the ligand-binding pockets of DRD2 (**a**), DRD3 (**b**, PDB code: 3PBL) and DRD4 (**c**, PDB code 5WIU) are shown in transparent grey. **d**, Schematic representation of risperidone-binding interactions at a 4.0 Å cut-off. Hydrogen bonds are shown as grey dashed lines. The red boxes indicate amino acids that, when mutated, reduce risperidone binding affinity by more than tenfold. The thermo-stabilizing mutation ($I122^{3.40}A$) is shown in blue. The deeper hydrophobic pocket is outlined in orange.

This construct was purified and crystallized in complex with the atypical antipsychotic risperidone. The binding affinities of multiple antipsychotics with this DRD2 construct were similar to those with the wild-type receptor (Extended Data Table 1), suggesting that the alterations that facilitate crystallization do not substantially perturb ligand binding. The crystal structure of the DRD2–risperidone complex was determined at 2.9 Å resolution (Extended Data Table 2 and Extended Data Fig. 1c–h).

Compared with DRD4 (Protein Data Bank (PDB) codes: 5WIU and 5WIV) and DRD3 (PDB code: 3PBL), DRD2 displays substan-tial structural differences in extracellular loop (EL)1 and EL2, and in the extracellular ends of transmembrane helices (TM)V, TMVI and TMVII (Fig. 1a–c). Unlike in DRD3 and DRD4, the largest extracel-lular loop of DRD2, EL2, extends away from the top of the receptor core (Fig. 1c). Notably, the highly conserved hydrophobic residue of EL2, which is two residues away from the conserved cysteine of EL2 in all extant aminergic GPCR structures and is represented by Ile184 in DRD2, points towards the receptor core (Extended Data Fig. 2). This residue has been implicated in the on-and-off-rate kinetics and in β-arrestin-biased signalling for some ligands at DRD2 and other receptors[19–21]. However, because of the rearrangement of EL2 and its formation of a small helical turn (residues 182–185) in the DRD2–risperidone structure (Fig. 1c and Extended Data Fig. 2c), and unlike the analogous residues in some aminergic receptor structures, Ile184 does not directly interact with the ligand (Extended Data Fig. 2a–l). Instead, Ile184 points across the binding pocket to interact with Trp100 in EL1, forming a hydrophobic network near the opening of the binding pocket (Extended Data Fig. 2m). We note that interactions between T4L and EL1 and EL2 in the crystal lattice may further stabilize this conformation (Extended Data Fig. 1c–e), but these weak interactions are unlikely to induce it.

DRD2 also differs from the other two D2-like dopamine receptors in that the extracellular tip of TMV is shifted towards the transmembrane bundle, while the extracellular tips of TMVI and TMVII are approximately 5.8 and 7.3 Å, and 1.4 and 2.1 Å further away from the receptor core, respectively, in comparison to the same regions in DRD3 and DRD4 (Fig. 1b). As in DRD3, an inter-helical hydrogen bond forms between $Tyr^{7.35}$ and $His^{6.55}$ (Extended Data Fig. 3a–d), which in DRD3 is important for regulating constitutive activity[17]. The side-chain conformations of DRD2, DRD3[16] and DRD4[17] residues $Tyr/Val^{7.35}$ and $His^{6.55}$ (Extended Data Fig. 3a–c) are also distinct[17]. Specifically, the side chain of $Tyr^{7.35}$ in DRD2 is rotated by 52° compared to the one in DRD3 to accommodate risperidone (Extended Data Fig. 3d). Together, these differences may further stabilize the outward movement of TMVI.

Like most antipsychotics, risperidone is a DRD2 inverse agonist[22], and therefore the DRD2–risperidone complex reflects an inactive state conformation. The most notable difference between active- and inactive-state GPCR structures is the extent to which the cytoplasmic tip of TMVI moves away from the transmembrane helical bundle to accommodate transducer binding[23]. A comparison of DRD2–risperidone with the active and inactive β_2 adrenergic receptor (β2AR) or adenosine A_{2A} receptor (A2AR) structures reveals no substantial outward movement of the intracellular end of TMVI (Extended Data Fig. 3e, f), a finding consistent with an inactive-state structure. Another important structural feature of GPCR activation is the rearrangement of side chains in the highly conserved microswitches D(E)/RY (TMIII) and NPXXY (TMVII)[23]. Here, Tyr$^{7.53}$ from the NPXXY motif and Arg$^{3.50}$ from the DRY motif adopt almost identical positions with homologous residues in the β2AR and A2AR inactive structures (Extended Data Fig. 3g–j). Moreover, a key inactive-state salt-bridge interaction, the 'ionic lock' between the conserved Arg$^{3.50}$ and Glu$^{6.30}$ (refs 24–26) is maintained in the DRD2–risperidone structure (Fig. 1d).

The benzisoxazole risperidone[27] displays a unique mode of dopamine receptor binding in comparison to those of the substituted benzamides eticlopride to DRD3 and nemonapride to DRD4 (Fig. 2). The benzisoxazole moiety of risperidone extends into a deep binding pocket defined by the side chains of TMIII, TMV and TMVI (Fig. 2a, d), and interacts with Cys118$^{3.36}$, Thr119$^{3.37}$, Ser197$^{5.46}$, Phe198$^{5.47}$, Phe382$^{6.44}$, Phe390$^{6.52}$ and Trp386$^{6.48}$, which form a subpocket below the orthosteric site (Fig. 2d). Additionally, another hydrophobic pocket above the orthosteric site encloses the tetrahydropyridopyrimidinone moiety of risperidone, whereas Asp114$^{3.32}$ forms a salt bridge with the tertiary amine of risperidone (Fig. 2d). Alanine mutagenesis of many of these contact residues reduces the affinity of risperidone binding to DRD2 (Fig. 2d and Extended Data Table 3). In the DRD3 and DRD4 structures, neither eticlopride nor nemonapride engages this deeper hydrophobic pocket (Fig. 2b, c). Importantly, alanine substitutions of the equivalent residues in this deeper hydrophobic pocket do not substantially alter [^{3}H]-nemonapride binding affinity for the DRD3 and the DRD4 receptors, except for Trp386$^{6.48}$ and Phe390$^{6.52}$, which are large enough that mutagenesis-induced alterations in helical packing alone might explain the observed effects (Extended Data Table 3).

Comparison of the overall ligand-binding pocket of DRD2 with structures of DRD3 and DRD4 revealed marked differences around residues Val/Phe$^{2.61}$, Trp^{EL1}, Phe/Leu$^{3.28}$ and Tyr/Val$^{7.35}$, which help to define an extended binding pocket (EBP) in DRD2 (Fig. 3a, b). Indeed, previous studies[16,17] on DRD3 and DRD4 revealed a selective EBP in each receptor. The DRD3 EBP is formed by the junction of EL1 and EL2 and the interface of TMII, TMIII and TMVII, and extends towards EL1 (Fig. 3c). By contrast, the DRD4 EBP reaches deep into a cleft between TMII and TMIII, defined by Phe91$^{2.61}$ and Leu111$^{3.28}$ (Fig. 3d); the structural determination of this DRD4 EBP enabled the structure-based discovery of agonists that are highly specific for this

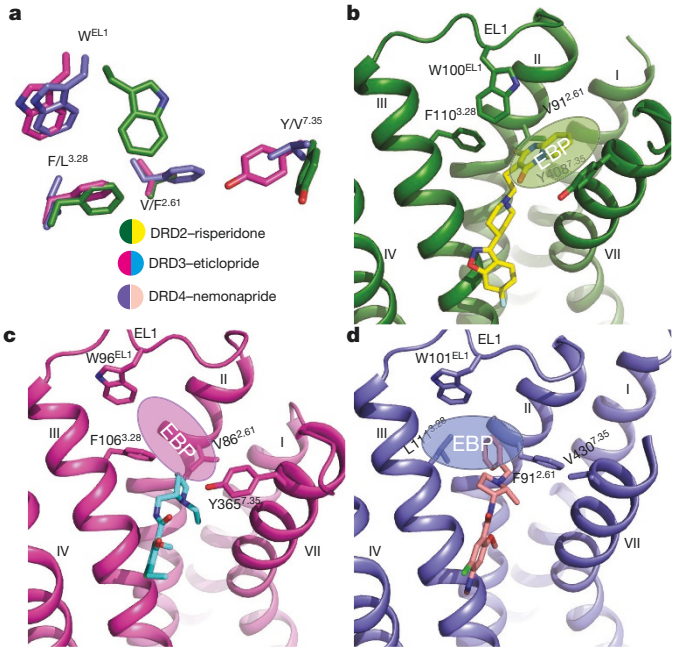

Figure 3 | Different extended binding pockets revealed across D2-like family receptors. a, The residues of DRD2 (green), DRD3 (pink, PDB code: 3PBL) and DRD4 (blue, PDB code: 5WIU) that define the extended binding pockets (EBPs) are shown as sticks. **b**–**d**, The distinctive selective EBPs in the D2-like family receptors DRD2 (**b**), DRD3 (**c**) and DRD4 (**d**). Residues and ligands are coloured as in **a**. The position of each EBP is shown as an ellipse.

receptor[17]. Unlike DRD3 or DRD4, the DRD2 EBP extends towards the extracellular part of TMVII, and is formed by EL1 and the junction of TMI, TMII and TMVII (Fig. 3b).

There are four distinctive features of the DRD2 EBP: (1) Compared to the DRD3 structure, part of the EL1 loop is rotated in DRD2, moving the conserved residue Trp^{EL1} to the top of the binding pocket (Fig. 3a–c and Extended Data Fig. 4), thereby disrupting what would be the DRD3 EBP (Fig. 3a–c). To our knowledge, this conformation of Trp^{EL1} is unique among aminergic receptor structures (Extended Data Fig. 4). (2) The phenylalanine residue is located at 3.28 in DRD2, rather than 2.61 in DRD4, which eliminates the equivalent of the extended pocket of DRD4 in DRD2 (Fig. 3a, b, d). (3) The Tyr408$^{7.35}$ side chain rotates towards the His393$^{6.55}$ side chain in DRD2, thereby avoiding clashing with risperidone (Extended Data Fig. 3a, d). (4) Finally, an outward movement of the extracellular tip of TMVII (Fig. 1b) makes additional space for the DRD2 EBP.

In comparison with the conformation adopted by risperidone when crystallized in isolation[4], risperidone's tetrahydropyridopyrimidinone

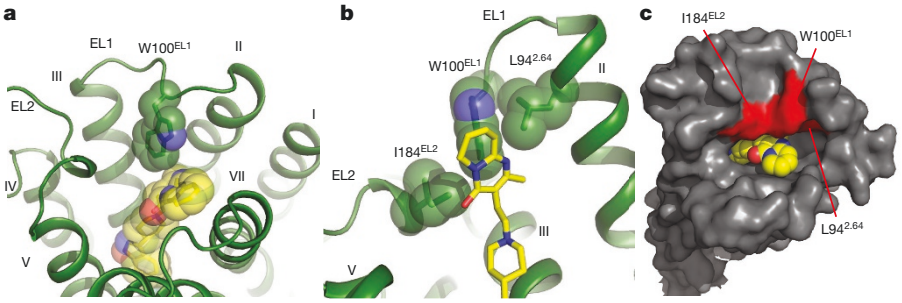

Figure 4 | The hydrophobic 'patch' of the DRD2 binding pocket. **a**, Risperidone (yellow) bound to the orthosteric pocket of DRD2 (green), viewed from the extracellular side. **b**, The W100^{EL1} side chain forms extensive hydrophobic contacts with residues L94$^{2.64}$ and I184^{EL2}. **c**, The residues L94$^{2.64}$, W 100^{EL1} and I184^{EL2} form a patch (red; residues outside the patch shown in grey) that narrows the binding pocket.

Table 1 | Risperidone dissociation and association rates with wild-type and mutant DRD2

Receptor	Residence time, min (k_{off} ± s.e.m, min^{-1})	k_{on} ± s.e.m. (M^{-1} min^{-1})	K_d (nM) (pK_d ± s.e.m.)
DRD2 wild-type	233 (0.0043 ± 0.0003)	$1.65 \times 10^6 \pm 1.7 \times 10^5$	2.51 (8.65 ± 0.21)
DRD2 $W100^{EL1}A$	28 (0.036 ± 0.0022) *P = 0.007	$5.63 \times 10^6 \pm 3.2 \times 10^5$	6.74 (8.17 ± 0.04)
DRD2 $W100^{EL1}L$	23 (0.043 ± 0.004) *P = 0.06	$6.32 \times 10^6 \pm 5.5 \times 10^5$	6.77 (8.17 ± 0.002)
DRD2 $W100^{EL1}F$	59 (0.017 ± 0.002) *P = 0.01	$3.12 \times 10^6 \pm 1.8 \times 10^5$	5.30 (8.28 ± 0.02)
DRD2 $L94^{2.64}A$	139 (0.0072 ± 0.0029) NS	$1.43 \times 10^7 \pm 2.3 \times 10^6$	0.48 (9.33 ± 0.12)
DRD2 $I184^{EL2}A$	185 (0.0054 ± 0.002) NS	$9.84 \times 10^6 \pm 1.4 \times 10^6$	0.54 (9.28 ± 0.10)
DRD2 $L94^{2.64}A/I184^{EL2}A$	6 (0.16 ± 0.05) *P = 0.005	$2.36 \times 10^7 \pm 7.8 \times 10^6$	7.01 (8.15 ± 0.02)

Data were acquired by association and dissociation kinetic experiments conducted in parallel at room temperature using [^{3}H]-*N*-methylspiperone (0.8–1.0 nM). Estimates of k_{off}, k_{on}, and K_d were obtained from four independent experiments. Residence time was calculated as $1/k_{off}$. All data are the mean ± s.e.m. of four independent assays (n = 4 independent experiments). Asterisks indicate statistically significant differences between wild-type and mutant receptors. NS, not significant; P values are indicated; unpaired two-tailed Student's t-test.

ring rotates by around 90° in the complex with DRD2 (Extended Data Fig. 5a). This ring interacts with a hydrophobic patch formed by the side chains of $Trp100^{EL1}$, $Ile184^{EL2}$, and $Leu94^{2.64}$. Although the electron density for $Leu94^{2.64}$ is weaker than for the other residues, the observed conformation of $Trp100^{EL1}$ appears to be stabilized by any rotamer of $Leu94^{2.64}$ that would fit the density.

In the DRD2–risperidone structure, the side chain of $Trp100^{EL1}$ forms extensive contacts with the tetrahydropyridopyrimidinone ring, wedging it into the DRD2 EBP (Figs. 3b, 4a and Extended Data Fig. 5b). In addition to these hydrophobic contacts between $Trp100^{EL1}$ and risperidone, $Trp100^{EL1}$ is also stabilized by contacts with $Ile184^{EL2}$ and, perhaps, $Leu94^{2.64}$, in spite of the lack of side chain electron density (Fig. 4b and Extended Data Fig. 5c). The observed configuration of risperidone is likely to be driven by the binding pocket of DRD2, and the conservation of key pocket residues such as $Trp100^{EL1}$ implies that risperidone could bind other aminergic receptors (for example, 5HT2A or the α1A adrenergic receptor) in a similar conformation, although further structures will be needed to test this notion.

Molecular docking of risperidone to homology models of DRD2, based on either the DRD3 or DRD4 structures, failed to reproduce the unique pose adopted by risperidone in the complex (Extended Data Fig. 5d–h). Rather, docking placed the ligand higher in the binding site, in a location analogous to that of eticlopride and nemonapride in the DRD3 and DRD4 structures, respectively (Fig. 2b, c). This is a direct consequence of the conformational rearrangements in DRD2 concomitant with accommodating risperidone—mainly movement of TMV, TMVI and TMVII, and the relocation of $Trp100^{EL1}$, which consequently affects the size and shape of the ligand-binding pocket, allowing risperidone to engage a deep binding pose and enter DRD2 EBP. Moreover, the docked conformation of risperidone resembles that of the receptor-free risperidone crystal structure[4], rather than the conformation adopted in the receptor-bound complex (Extended Data Fig. 5d–h). This is not a problem of conformational sampling on the part of docking—the receptor-free structure is, after all, a low energy structure, and docking captures this—but rather, it reflects the incorrect modelling of $Trp100^{EL1}$, owing to the lack of an analogous configuration in templates used in the modelling. Accordingly, docking does not predict the approximately 90° rotation of the tetrahydropyridopyrimidinone ring of risperidone in the DRD2 complex. The binding pocket of DRD2 and the unusual risperidone conformation that it accommodates are unexpected features of this structure, with implications for our understanding of ligand recognition by this receptor and for the design of new ligands to modulate its activity.

The rearrangement of the extracellular surface and movement of $Trp100^{EL1}$ in comparison to the DRD3 and DRD4 structures not only allows it to interact with risperidone, but also forms, together with $Ile184^{EL2}$ and $Leu94^{2.64}$, a hydrophobic patch that potentially narrows the binding pocket (Fig. 4b, c). We hypothesized that these residues prevent risperidone from exiting the binding pocket. We found that $Trp100^{EL1}$Phe, $Trp100^{EL1}$Leu and $Trp100^{EL1}$Ala mutations decreased risperidone residence time from 233 min in the wild-type receptor to 59, 23 and 28 min, respectively (Table 1 and Extended Data Fig. 6a–d). Notably, these kinetic effects of the $Trp100^{EL1}$Phe, $Trp100^{EL1}$Leu and $Trp100^{EL1}$Ala mutants on residence time were shared with other tested antipsychotics, including N-methylspiperone, nemonapride and aripiprazole (Extended Data Fig. 6h–k, o–p and Extended Data Table 4). Similarly, the $I184^{ECL2}A/L94^{2.64}A$ double mutation (Table 1 and Extended Data Fig. 6g) reduced the residence time of risperidone to 6 min, and also reduced the residence times of other antipsychotics (Table 1, Extended Data Fig. 6n, q, r and Extended Data Table 4). In summary, $L94^{2.64}$, $Trp100^{EL1}$ and $I184^{ECL2}$ form hydrophobic contacts that contribute to the slow dissociation of risperidone from DRD2.

Among the most serious side effects of antipsychotics are extrapyramidal symptoms (EPS). A consistent finding in patients with EPS is DRD2 occupancy of more than 80% in the central nervous system, as demonstrated by positron emission tomography (PET)[28]. It has been hypothesized that differential binding kinetics[29,30] and the relatively higher affinity of atypical antipsychotic drugs for 5HT2A serotonin receptors[3,4] contribute to the lower incidence of EPS with atypical antipsychotic drugs, such as risperidone, versus typical antipsychotics. We note that $Trp100^{EL1}$ regulates both the association and dissociation kinetics of risperidone, and that many of the residues that are essential for risperidone binding to DRD2 are shared with 5HT2A serotonin and other biogenic amine receptors. Thus, although our findings do not definitively resolve these hypotheses, they do provide the initial underpinnings for molecularly derived models of the actions of antipsychotic drugs at dopamine and other receptors. Finally, given recent successes in leveraging crystal structures of GPCRs for ligand discovery[17–19], we anticipate that the DRD2–risperidone complex structure will accelerate the search for novel antipsychotic drugs targeting DRD2.

Online Content Methods, along with any additional Extended Data display items and Source Data, are available in the online version of the paper; references unique to these sections appear only in the online paper.

Received 9 December 2017; accepted 18 January 2018.
Published online 24 January 2018.

1. Missale, C., Nash, S. R., Robinson, S. W., Jaber, M. & Caron, M. G. Dopamine receptors: from structure to function. *Physiol. Rev.* **78,** 189–225 (1998).
2. Creese, I., Burt, D. R. & Snyder, S. H. Dopamine receptor binding predicts clinical and pharmacological potencies of antischizophrenic drugs. *Science* **192,** 481–483 (1976).
3. Meltzer, H. Y., Matsubara, S. & Lee, J.-C. Classification of typical and atypical antipsychotic drugs on the basis of dopamine D-1, D-2 and serotonin2 p*Ki* values. *J. Pharmacol. Exp. Ther.* **251,** 238–246 (1989).
4. Roth, B. L., Sheffler, D. J. & Kroeze, W. K. Magic shotguns versus magic bullets: selectively non-selective drugs for mood disorders and schizophrenia. *Nat. Rev. Drug Discov.* **3,** 353–359 (2004).
5. Roth, B. L. Drugs and valvular heart disease. *N. Engl. J. Med.* **356,** 6–9 (2007).
6. Seeman, P. & Lee, T. Antipsychotic drugs: direct correlation between clinical potency and presynaptic action on dopamine neurons. *Science* **188,** 1217–1219 (1975).
7. Sibley, D. R. & Monsma, F. J. Jr. Molecular biology of dopamine receptors. *Trends Pharmacol. Sci.* **13,** 61–69 (1992).
8. Beaulieu, J. M. & Gainetdinov, R. R. The physiology, signaling, and pharmacology of dopamine receptors. *Pharmacol. Rev.* **63,** 182–217 (2011).
9. Volkow, N. D., Fowler, J. S., Wang, G. J., Swanson, J. M. & Telang, F. Dopamine in drug abuse and addiction: results of imaging studies and treatment implications. *Arch. Neurol.* **64,** 1575–1579 (2007).
10. Bunzow, J. R. *et al.* Cloning and expression of a rat D2 dopamine receptor cDNA. *Nature* **336,** 783–787 (1988).
11. Grandy, D. K. *et al.* Cloning of the cDNA and gene for a human D2 dopamine receptor. *Proc. Natl Acad. Sci. USA* **86,** 9762–9766 (1989).

12. Monsma, F. J., Jr, McVittie, L. D., Gerfen, C. R., Mahan, L. C. & Sibley, D. R. Multiple D2 dopamine receptors produced by alternative RNA splicing. *Nature* **342,** 926–929 (1989).
13. Allen, J. A. *et al.* Discovery of β-arrestin-biased dopamine D2 ligands for probing signal transduction pathways essential for antipsychotic efficacy. *Proc. Natl Acad. Sci. USA* **108,** 18488–18493 (2011).
14. Javitch, J. A., Fu, D., Chen, J. & Karlin, A. Mapping the binding-site crevice of the dopamine D2 receptor by the substituted-cysteine accessibility method. *Neuron* **14,** 825–831 (1995).
15. Ballesteros, J. A., Shi, L. & Javitch, J. A. Structural mimicry in G protein-coupled receptors: implications of the high-resolution structure of rhodopsin for structure-function analysis of rhodopsin-like receptors. *Mol. Pharmacol.* **60,** 1–19 (2001).
16. Chien, E. Y. *et al.* Structure of the human dopamine D3 receptor in complex with a D2/D3 selective antagonist. *Science* **330,** 1091–1095 (2010).
17. Wang, S. *et al.* D4 dopamine receptor high-resolution structures enable the discovery of selective agonists. *Science* **358,** 381–386 (2017).
18. Manglik, A. *et al.* Structure-based discovery of opioid analgesics with reduced side effects. *Nature* **537,** 185–190 (2016).
19. Wacker, D., Stevens, R. C. & Roth, B. L. How ligands illuminate GPCR molecular pharmacology. *Cell* **170,** 414–427 (2017).
20. McCorvy, J. D. *et al.* Structure-inspired design of β-arrestin-biased ligands for aminergic GPCRs. *Nat. Chem. Biol.* **14,** 126–134 (2018).
21. Free, R. B. *et al.* Discovery and characterization of a G protein-biased agonist that inhibits β-arrestin recruitment to the D2 dopamine receptor. *Mol. Pharmacol.* **86,** 96–105 (2014).
22. Roberts, D. J. & Strange, P. G. Mechanisms of inverse agonist action at D2 dopamine receptors. *Br. J. Pharmacol.* **145,** 34–42 (2005).
23. Rasmussen, S. G. *et al.* Crystal structure of the β_2 adrenergic receptor-G_s protein complex. *Nature* **477,** 549–555 (2011).
24. Shapiro, D. A., Kristiansen, K., Weiner, D. M., Kroeze, W. K. & Roth, B. L. Evidence for a model of agonist-induced activation of 5–HT2A serotonin receptors which involves the disruption of a strong ionic interaction between helices 3 and 6. *J. Biol. Chem.* **18,** 11441–11449 (2002).
25. Ballesteros, J. A. *et al.* Activation of the β_2-adrenergic receptor involves disruption of an ionic lock between the cytoplasmic ends of transmembrane segments 3 and 6. *J. Biol. Chem.* **276,** 29171–29177 (2001).
26. Palczewski, K. *et al.* Crystal structure of rhodopsin: a G protein-coupled receptor. *Science* **289,** 739–745 (2000).
27. Janssen, P. A. *et al.* Pharmacology of risperidone (R 64 766), a new antipsychotic with serotonin–S2 and dopamine–D2 antagonistic properties. *J. Pharmacol. Exp. Ther.* **244,** 685–693 (1988).
28. Kapur, S., Zipursky, R., Jones, C., Remington, G. & Houle, S. Relationship between dopamine D2 occupancy, clinical response, and side effects: a double-blind PET study of first-episode schizophrenia. *Am. J. Psychiatry* **157,** 514–520 (2000).
29. Kapur, S. & Seeman, P. Does fast dissociation from the dopamine D2 receptor explain the action of atypical antipsychotics?: A new hypothesis. *Am. J. Psychiatry* **158,** 360–369 (2001).
30. Sykes, D. A. *et al.* Extrapyramidal side effects of antipsychotics are linked to their association kinetics at dopamine D2 receptors. *Nat. Commun.* **8,** 763 (2017).

Supplementary Information is available in the online version of the paper.

Acknowledgements This work was supported by NIH Grants RO1MH61887, U19MH82441, the NIMH Psychoactive Drug Screening Program Contract and the Michael Hooker Chair for Protein Therapeutics and Translational Proteomics (to B.L.R.) and by R35GM122481 (to B.K.S.). We thank J. Sondek and S. Endo-Streeter for providing independent structure quality control analysis; M. J. Miley and the UNC macromolecular crystallization core for advice and use of their equipment for crystal harvesting and transport, which is supported by the National Cancer Institute under award number P30CA016086; B. E. Krumm for advice on data processing and help with thermostabilization assays; and the staff of GM/CA@APS, which has been funded with Federal funds from the National Cancer Institute (ACB-12002) and the National Institute of General Medical Sciences (AGM-12006). This research used resources of the Advanced Photon Source, a US Department of Energy (DOE) Office of Science user facility operated for the DOE Office of Science by Argonne National Laboratory under Contract No. DE-AC02-06CH11357.

Author Contributions S.W. designed experiments, developed the DRD2 construct and purification, expressed, purified and crystallized the receptor, collected diffraction data, solved and refined the structure, analysed the structure, performed radioligand binding and prepared the manuscript. T.C. performed radioligand binding, analysed the data and assisted with preparing the manuscript. A.L. conducted the homology modelling and docking and helped to edit the manuscript. B.K.S. supervised the modelling and docking and helped to prepare the manuscript. D.W. refined and analysed the structure, supervised the structure determination and assisted with preparing the manuscript. B.L.R. supervised the overall project and management and prepared the manuscript.

Author Information Reprints and permissions information is available at www.nature.com/reprints. The authors declare no competing financial interests. Readers are welcome to comment on the online version of the paper. Publisher's note: Springer Nature remains neutral with regard to jurisdictional claims in published maps and institutional affiliations. Correspondence and requests for materials should be addressed to S.W. (shengunc@email.unc.edu), D.W. (dwacker@email.unc.edu) and B.L.R. (bryan_roth@med.unc.edu).

Reviewer Information *Nature* thanks D. Sibley and the other anonymous reviewer(s) for their contribution to the peer review of this work.

METHODS

Protein engineering for structural studies. To facilitate expression, purification, and crystallography, a human DRD2 (D2 long receptor variant[12]) construct was generated with several modifications. T4L residues 2–161[31] were fused into the third intracellular loop of DRD2 (V223–R361) with truncations of the N-terminal residues 1–34. The DRD2-T4L construct was further modified by introducing three mutations I122$^{3.40}$A, L375$^{6.37}$A and L379$^{6.41}$A, identified by alanine scanning, to improve protein thermostability. In brief, alanine scanning was used to identify thermostabilization mutations (see 'Radioligand binding assay' for details; Extended Data Fig. 1a). The chimeric receptor sequences were then subcloned into a modified pFastBac1 vector (Invitrogen), designated pFastBac1-833100, which contained an expression cassette with a haemagglutinin signal sequence followed by a Flag tag, a 10×His tag and a TEV protease recognition site at the N terminus before the receptor sequence.

Protein expression and purification. The modified DRD2-T4L protein was expressed in *Spodoptera frugiperda* (Sf9) cells (Expression Systems) using the Bac-to-Bac Baculovirus Expression System (Invitrogen) for 48 h. The insect cells were lysed by repeated washing and centrifugation in hypotonic buffer with low (10 mM HEPES, pH 7.5, 10 mM $MgCl_2$, 20 mM KCl and EDTA-free complete protease inhibitor cocktail tablets (Roche)) (once) and high (1.0 M NaCl, 10 mM HEPES, pH 7.5, 10 mM $MgCl_2$, 20 mM KCl) salt concentration (three times). The washed membranes were suspended in buffer containing 10 mM HEPES, pH 7.5, 10 mM $MgCl_2$, 20 mM KCl, 150 mM NaCl, 20 μM risperidone and EDTA-free complete protease inhibitor cocktail tablets, incubated at room temperature for 1 h and then incubated at 4 °C for 30 min before solubilization. The membranes were then solubilized in 10 mM HEPES, pH 7.5, 150 mM NaCl, 1% (wt/vol) *n*-dodecyl-β-D-maltopyranoside (DDM, Anatrace), 0.2% (wt/vol) cholesteryl hemisuccinate (CHS, Sigma) for 2 h at 4 °C.

The supernatant was isolated by centrifugation at 150,000 *g* for 30 min, followed by incubation in 20 mM buffered imidazole (pH 7.5) and 800 mM NaCl with TALON IMAC resin (Clontech) at 4 °C overnight. The resin was then washed with 10 column volumes of Wash Buffer I (50 mM HEPES, pH 7.5, 800 mM NaCl, 0.1% (wt/vol) DDM, 0.02% (wt/vol) CHS, 20 mM imidazole, 10% (vol/vol) glycerol and 10 μM risperdone), followed by 10 column volumes of Wash Buffer II (25 mM HEPES, pH 7.5, 150 mM NaCl, 0.05% (wt/vol) DDM, 0.01% (wt/vol) CHS, 10% (vol/vol) glycerol and 10 μM risperidone). The protein was then eluted in 3–4 column volumes of Elution Buffer (50 mM HEPES (pH 7.5), 50 μM risperidone, 500 mM NaCl, 10% (vol/vol) glycerol, 0.05% (wt/vol) DDM, 0.01% (wt/vol) CHS, and 250 mM imidazole). A PD MiniTrap G-25 column (GE Healthcare) was used to remove imidazole. The protein was then treated overnight with His-tagged TEV protease and His-tagged PNGase F (NEB) to remove the N-terminal His tag and Flag-tag, and to deglycosylate the receptor. His-tagged TEV protease, His-tagged PNGase F, cleaved His-tag and uncleaved protein were removed from the sample by passing the sample over equilibrated TALON IMAC resin (Clontech). The receptor was then concentrated to 40–50 mg ml^{-1} with a 100 kDa molecular mass cut-off Vivaspin 500 centrifuge concentrator (Sartorius Stedim).

Lipidic cubic-phase crystallization. Protein samples of DRD2 in complex with risperidone were reconstituted into the lipidic cubic phase (LCP) by mixing 40% of ~60 mg ml^{-1} purified DRD2–risperidone with 60% lipid (10% (wt/wt) cholesterol, 90% (wt/wt) monoolein) using the twin-syringe method[32]. Crystallization trials were performed in glass sandwich plates (Marienfeld) using a handheld dispenser (Art Robbins Instruments), dispensing 50 nl of protein-laden LCP and 1 μl precipitant solution per well. Plates were then incubated at 20 °C. Crystals were obtained from precipitant conditions containing 100 mM Tris/HCl pH 7.8, 230 mM lithium nitrate, 25% PEG400, 4% (±)1,3-butanediol. Crystals grew to maximum size of 40 μm × 40 μm × 10 μm within two weeks and were harvested directly from the LCP matrix using MiTeGen micromount loops and flash frozen in liquid nitrogen.

Data collection, structure solution and refinement. Crystallographic diffraction data collection was performed at the 23ID-B and 23ID-D beamlines (GM/CA CAT) at the Advanced Photon Source, Argonne, Illinois using a 10-μm minibeam at a wavelength of 1.0330 Å and a Dectris Eiger-16m or Pilatus3 6M detector, respectively. The crystals were exposed to 0.5 s of unattenuated beam using 0.5° oscillation per frame. A 97.3% complete data set at 2.90 Å resolution of DRD2–risperidone from 20 crystals was integrated, scaled and merged using HKL3000[33]. Initial phase information was obtained by molecular replacement with the program PHASER[34] using two independent search models: a receptor portion of the DRD4–nemonapride complex (PDB code: 5WIU), and the T4L portion of β2AR–T4L (PDB code: 2RH1) as initial models. Refinement was performed with PHENIX[35] and REFMAC followed by manual examination and rebuilding of the refined coordinates in the program COOT[36] using $|2F_o|-|F_c|$, $|F_o|-|F_c|$, and omit maps.

Radioligand-binding assay. Binding assays were performed using membrane fractions of Sf9 cells expressing the crystallization construct DRD2–T4L (I122$^{3.40}$A, L375$^{6.37}$A and L379$^{6.41}$A) or membrane preparations of HEK-293T transiently expressing DRD2 (D2 long receptor) and different mutants. HEK-293T cells (ATCC CRL-11268; 59587035; mycoplasma free) were transfected and membrane preparation and radioligand binding assays were set up in 96-well plates as described previously[13]. All binding assays were conducted in standard binding buffer (50 mM Tris, 10 mM $MgCl_2$, 0.1 mM EDTA, 0.1% BSA, pH 7.4). For displacement experiments, increasing concentrations of compounds were incubated with membrane and radioligands (0.8–1.0 nM [^{3}H]-*N*-methylspiperone or 0.1–0.5 nM [^{3}H]-nemonapride) (PerkinElmer) for 2 h at room temperature in the dark. To determine the affinity of nemonapride for DRD2 and different mutants, all assays used at least two concentrations of [^{3}H]-nemonapride. The reaction was terminated by rapid vacuum filtration onto chilled 0.3% PEI-soaked GF/A filters followed by three quick washes with cold washing buffer (50 mM Tris HCl, pH 7.4) and quantified as described previously[8]. Results (with or without normalization) were analysed using GraphPad Prism using one-site shift models where indicated.

Radioligand-based thermostability assay. Membranes from HEK-293T cells expressing wild-type or mutant human DRD2 were resuspended in binding buffer (50 mM Tris, 10 mM $MgCl_2$, 0.1 mM EDTA, 0.1% BSA, pH 7.4). [^{3}H]-*N*-methylspiperone was added to the membranes to give a final concentration of 1 nM. The samples were incubated at room temperature for 1 h and then aliquoted into PCR strips. Samples were heated to the desired temperature for exactly 30 min, then cooled down to 25 °C for 30 min. The samples were terminated by rapid vacuum filtration onto chilled 0.3% PEI-soaked GF/A filters followed by three quick washes with cold washing buffer (50 mM Tris HCl, pH 7.4) and quantified as described previously[8]. Results were analysed using GraphPad Prism. Apparent T_m values were derived from sigmoidal dose–response analysis. Results represent the mean ± s.e.m. of three independent experiments.

Differential-scanning fluorimetry-based thermostability assay. The thermal stability of purified protein was determined by measuring fluorescence of the thiol-reactive dye BODIPY FL L-cystine (Invitrogen). The standard assay conditions were 20 mM HEPES (pH 7.5), 200 mM NaCl, 0.025% DDM and 10 mM risperidone with protein concentrations of 1 mg ml^{-1} and 1 μM BODIPY FL L-cystine. The melting experiments were performed on a StepOnePlus real-time PCR system from Applied Biosystems. The melting curve experiments were conducted (1 °C/min) and recorded using StepOne software from Applied Biosystems. Results were analysed using GraphPad Prism. Apparent T_m values were derived from sigmoidal dose–response analysis. Results represent the mean ± s.e.m. of three independent experiments.

Ligand association and dissociation radioligand-binding assays. Binding assays were performed using membrane preparations of HEK-293T cells transiently expressing DRD2 (D2 long receptor) and different mutants at room temperature. Radioligand dissociation and association assays were performed in parallel using the same concentrations of radioligand, membrane preparations and binding buffer (50 mM Tris, 10 mM $MgCl_2$, 0.1 mM EDTA, 0.1% BSA, pH 7.4). All assays used at least two concentrations of radioligand (0.5–1.0 nM [^{3}H]-*N*-methylspiperone; 0.5–2.0 nM [^{3}H]-nemonapride). For dissociation assays, membranes were incubated with radioligand for at least 2 h at room temperature before the addition of 10 μl of 10 μM excess cold ligand to the 200 μl membrane suspension at designated time points. For association experiments, 100 μl of radioligand was added to 100 μl membrane suspensions at designated time points. Time points spanned 1 min to 7 h, depending on experimental conditions and radioligand. For the determination of k_{on} and k_{off} for unlabelled risperidone or aripiprazole, membranes containing either wild-type or mutant proteins were incubated with [^{3}H]-methylspiperone and several concentrations of risperidone or aripiprazole. Non-specific binding was determined by addition of 10 μM nemonapride. Immediately (at time = 0 min), plates were harvested by vacuum filtration onto 0.3% polyethyleneimine pre-soaked 96-well filter mats (Perkin Elmer) using a 96-well Filtermate harvester, followed by three washes with cold wash buffer (50 mM Tris pH 7.4). Scintillation cocktail (Meltilex, Perkin Elmer) was melted onto dried filters and radioactivity was counted using a Wallac Trilux MicroBeta counter (PerkinElmer). Data were analysed using 'dissociation-one phase exponential decay' or 'association kinetics-two or more concentrations of hot radioligand' in Graphpad Prism 5.0. The previously determined [^{3}H]-*N*-methylspiperone k_{on} and k_{off} rates of DRD2 or mutants were used to estimate the k_{on} and k_{off} rates of risperidone and aripiprazole using the 'kinetics of competitive binding' equation in Graphpad Prism 5.0 as proposed[37].

Homology modelling of DRD2. Sequence alignment for construction of the DRD2 homology models was generated with PROMALS3D[38], using sequences of human DRD2 (Uniprot accession number: P14416), DRD3 (P35462) and DRD4 (P21917), as well as sequences of available DRD2-family X-ray structures (DRD3, PDB code: 3PBL (chain A)[16] and DRD4, PDB code: 5WIU (chain A)[17]). The

alignment was manually edited to remove the amino and carboxy termini which extended past the template structures, and to remove the engineered T4 lysozyme (PDB code: 3PBL) or apocytochrome b562 RIL (BRIL, PDB code: 5WIU) from the template sequences on DRD4. MODELLER-9v15[39] was then used to generate (1) a total of 1,000 homology models of DRD2, based on the crystal structure of DRD4 in complex with nemonapride as the template, and (2) a set of 500 models based on the crystal structure of DRD3 in complex with eticlopride. We then evaluated the models for their ability to enrich known DRD2 ligands over property-matched decoys through docking to the orthosteric binding site, using DOCK 3.7[40] (as detailed below). While sharing physical properties of known ligands, decoy molecules are topologically distinct and so unlikely to bind the receptor, thus controlling for the enrichment of molecules by physical properties alone. Thirty-two known DRD2 antagonists with molecular weight $<$420 were extracted from the IUPHAR database[41], and 1,836 property-matched decoys were generated using the DUD-E server[42]. The models were then ranked on the basis of their adjusted logAUC. The selected best-scoring model in terms of ligand enrichment was further optimized through minimization with the AMBER protein force field and the GAFF ligand force field supplemented with AM1BCC charges[43].

Molecular docking of risperidone. Risperidone was docked to the orthosteric binding site of the DRD2 homology models based on the DRD3 or DRD4 crystal structures using DOCK3.7[40]. DOCK3.7 places pre-generated flexible ligands into the binding site by superimposing atoms of each molecule on matching spheres, representing favourable positions for individual ligand atoms. Forty-five matching spheres were used, based on the pose of the corresponding X-ray ligand (eticlopride or nemonapride) in the template structure. The resulting docked ligand poses were scored by summing the receptor–ligand electrostatics and van der Waals interaction energies, and corrected for context-dependent ligand desolvation. Receptor structures were protonated using Reduce[44]. Partial charges from the united-atom AMBER[43] force field were used for all receptor atoms. Grids that evaluate the different energy terms of the DOCK scoring function were precalculated using AMBER[43] for the van der Waals term, QNIFFT[45,46] (an adaptation of DELPHI) for electrostatics, and ligand desolvation[47]. Ligands were protonated with Marvin (v15.11.23.0, ChemAxon, 2015; http://www.chemaxon.com), at pH 7.4. Each protomer was rendered into 3D using Corina[48] (Molecular Networks) and conformationally sampled using Omega[49] (OpenEye Scientific Software). Ligand charges and initial solvation energies were calculated using AMSOL[50,51].

Data availability. Atomic coordinates and structure factor files for the DRD2–Risperidone structure have been deposited in the RCSB Protein Data Bank with identification code 6C38. All other data are available from the corresponding authors upon reasonable request.

31. Rosenbaum, D. M. *et al.* GPCR engineering yields high-resolution structural insights into β_2-adrenergic receptor function. *Science* **318,** 1266–1273 (2007).
32. Caffrey, M. & Cherezov, V. Crystallizing membrane proteins using lipidic mesophases. *Nat. Protocols* **4,** 706–731 (2009).
33. Minor, W., Cymborowski, M., Otwinowski, Z. & Chruszcz, M. HKL-3000: the integration of data reduction and structure solution—from diffraction images to an initial model in minutes. *Acta Crystallogr. D Biol. Crystallogr.* **62,** 859–866 (2006).
34. McCoy, A. J. *et al.* Phaser crystallographic software. *J. Appl. Crystallogr.* **40,** 658–674 (2007).
35. Adams, P. D. *et al.* PHENIX: a comprehensive Python-based system for macromolecular structure solution. *Acta Crystallogr. D Biol. Crystallogr.* **66,** 213–221 (2010).
36. Emsley, P., Lohkamp, B., Scott, W. G. & Cowtan, K. Features and development of Coot. *Acta Crystallogr. D Biol. Crystallogr.* **66,** 486–501 (2010).
37. Motulsky, H. J. & Mahan, L. C. The kinetics of competitive radioligand binding predicted by the law of mass action. *Mol. Pharmacol.* **25,** 1–9 (1984).
38. Pei, J. & Grishin, N. V. PROMALS3D: multiple protein sequence alignment enhanced with evolutionary and three-dimensional structural information. *Methods Mol. Biol.* **1079,** 263–271 (2014).
39. Webb, B. & Sali, A. Comparative protein structure modeling using MODELLER. *Curr. Protoc. Bioinformatics* **47,** 5 6 1–5 6 32 (2014).
40. Coleman, R. G., Carchia, M., Sterling, T., Irwin, J. J. & Shoichet, B. K. Ligand pose and orientational sampling in molecular docking. *PLoS One* **8,** e75992 (2013).
41. Southan, C. *et al.* The IUPHAR/BPS Guide to pharmacology in 2016: towards curated quantitative interactions between 1300 protein targets and 6000 ligands. *Nucleic Acids Res.* **44** (D1), D1054–D1068 (2016).
42. Mysinger, M. M., Carchia, M., Irwin, J. J. & Shoichet, B. K. Directory of useful decoys, enhanced (DUD-E): better ligands and decoys for better benchmarking. *J. Med. Chem.* **55,** 6582–6594 (2012).
43. Case, D. A. *et al.* AMBER 2015. (University of California, 2015).
44. Word, J. M., Lovell, S. C., Richardson, J. S. & Richardson, D. C. Asparagine and glutamine: using hydrogen atom contacts in the choice of side-chain amide orientation. *J. Mol. Biol.* **285,** 1735–1747 (1999).
45. Gallagher, K. & Sharp, K. Electrostatic contributions to heat capacity changes of DNA-ligand binding. *Biophys. J.* **75,** 769–776 (1998).
46. Sharp, K. A. Polyelectrolyte electrostatics: Salt dependence, entropic, and enthalpic contributions to free energy in the nonlinear Poisson–Boltzmann model. *Biopolymers* **36,** 227–243 (1995).
47. Mysinger, M. M. & Shoichet, B. K. Rapid context-dependent ligand desolvation in molecular docking. *J. Chem. Inf. Model.* **50,** 1561–1573 (2010).
48. Sadowski, J., Gasteiger, J. & Klebe, G. Comparison of automatic three-dimensional model builders using 639 X-ray structures. *J. Chem. Inf. Comput. Sci.* **34,** 1000–1008 (1994).
49. Hawkins, P. C., Skillman, A. G., Warren, G. L., Ellingson, B. A. & Stahl, M. T. Conformer generation with OMEGA: algorithm and validation using high quality structures from the Protein Databank and Cambridge Structural Database. *J. Chem. Inf. Model.* **50,** 572–584 (2010).
50. Chambers, C. C., Hawkins, G. D., Cramer, C. J. & Truhlar, D. G. Model for aqueous solvation based on class IV atomic charges and first solvation shell effects. *J. Phys. Chem.* **100,** 16385–16398 (1996).
51. Li, J., Zhu, T., Cramer, C. J. & Truhlar, D. G. New class IV charge model for extracting accurate partial charges from wave functions. *J. Phys. Chem. A* **102,** 1820–1831 (1998).

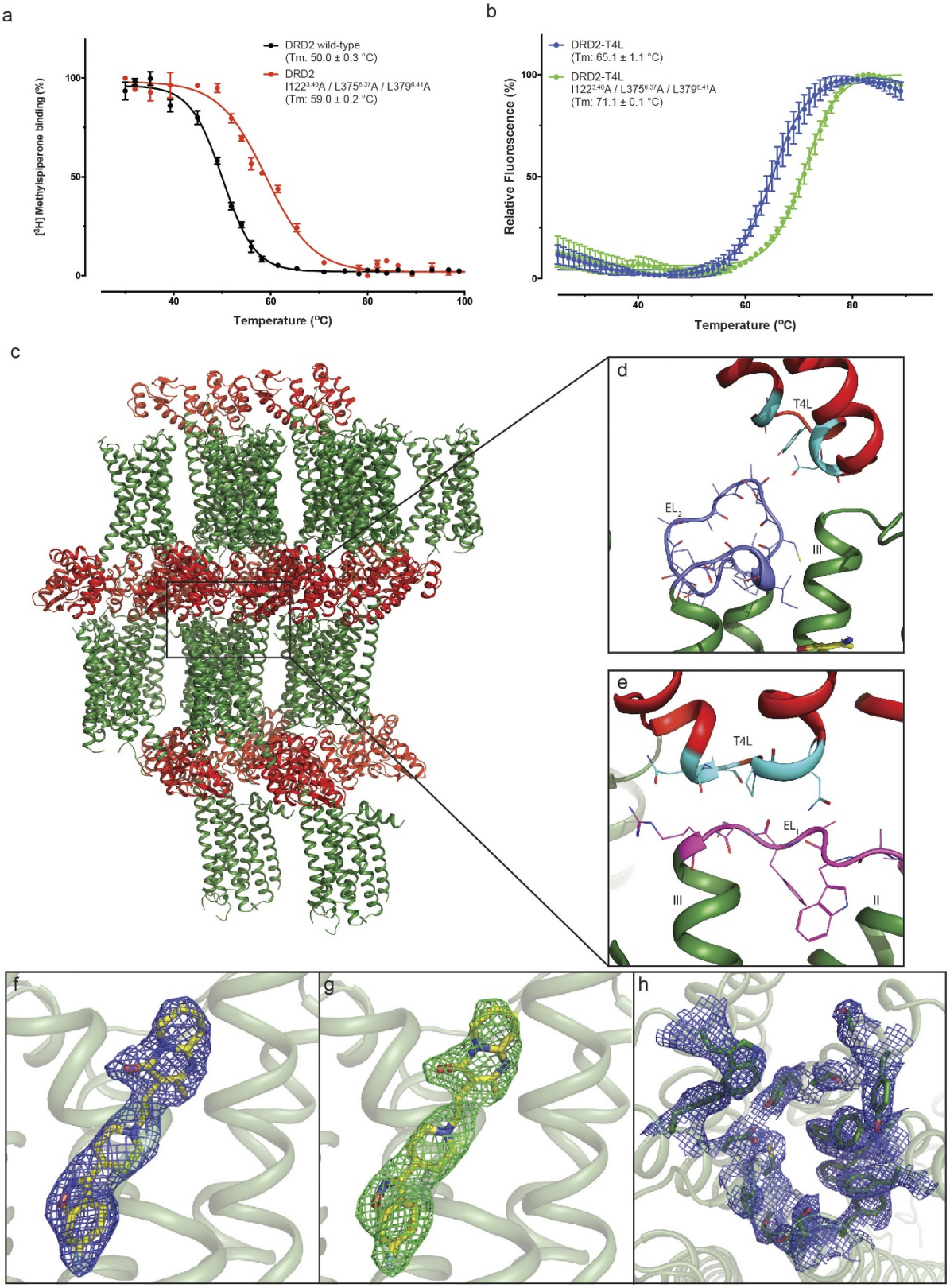

Extended Data Figure 1 | Thermostability of DRD2 constructs, crystal packing of the DRD2–risperidone complex and representative electron density of the DRD2 structure. a, Membranes containing DRD2 or DRD2 with thermostability mutations were heated for 30 min with 1 nM [^{3}H]-*N*-methylspiperone and the amount of bound [^{3}H]-ligand was determined. **b**, Purified DRD2–T4L protein (with or without thermostability mutations) was heated with 10 μM risperidone and 1 μM BODIPY FL L-cystine dye using a temperature gradient and the amount of dye bound to unfolding protein was determined. Data were analysed by nonlinear regression and apparent T_m values (transition temperature where 50% of the receptor is inactive) were determined from analysis of the sigmoidal melting curves. All data in **a** and **b** are mean ± s.e.m. of three independent assays. **c**–**e**, Packing of the DRD2–risperidone complex crystallized in the $P2_12_12_1$ spacegroup. DRD2 is shown in green and the T4L-fusion protein is shown in red, or in cyan where it interacts with DRD2. EL1 and EL2 of DRD2 are shown in magenta and blue, respectively. **f**, $2F_o$–F_c electron density map (blue mesh) of risperidone (yellow) contoured at 1σ. **g**, F_o–F_c omit map (green mesh) contoured at 3.0σ of risperidone (yellow). **h**, 2 F_o–F_c electron density map of DRD2 binding pocket residues (blue mesh) contoured at 1σ.

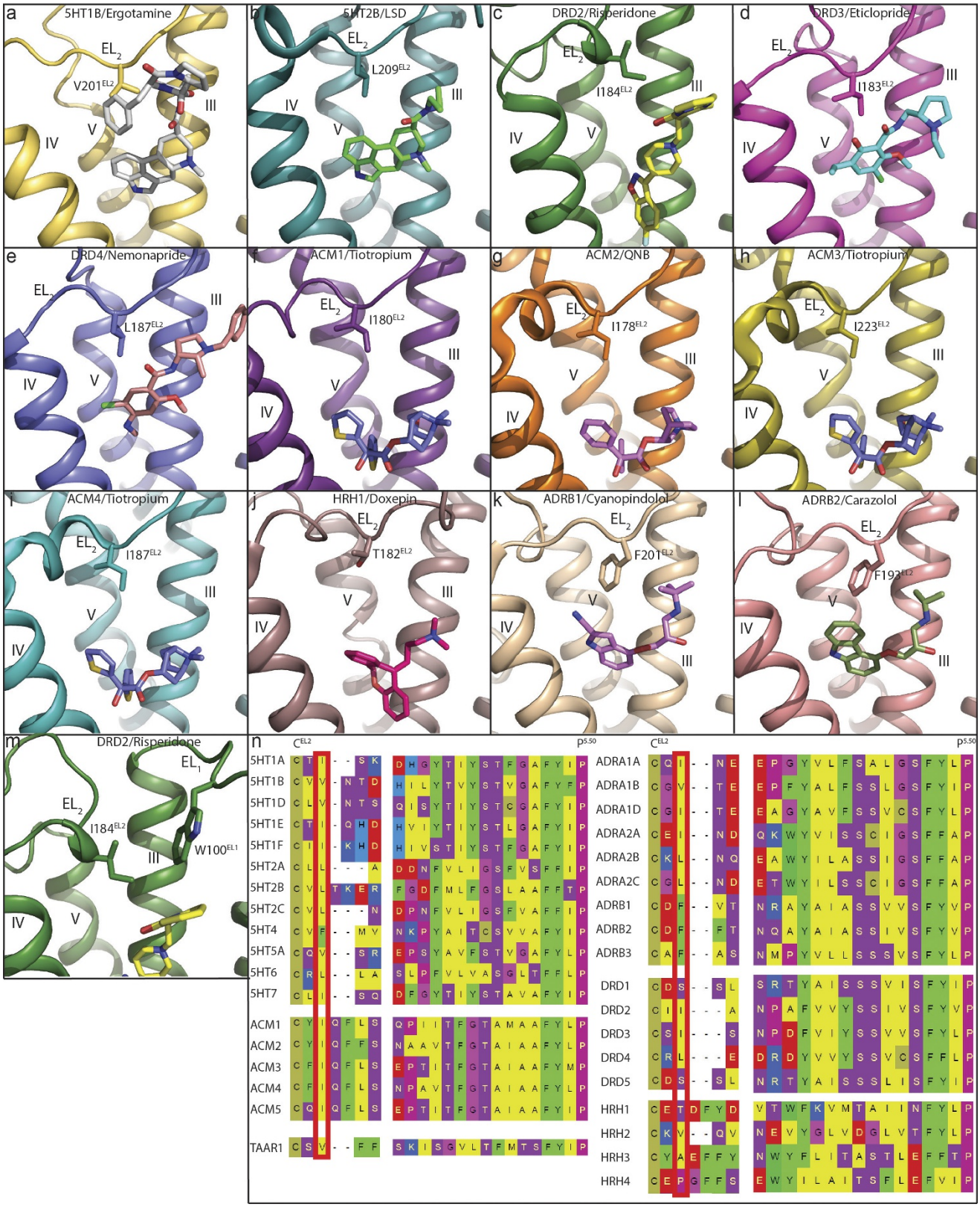

Extended Data Figure 2 | Conserved hydrophobic residue of EL2 in all available aminergic receptor structures. In all panels, receptors are shown as cartoons. Ligands and residues are shown as sticks. **a**, 5HT1B (PDB code: 4IAR). **b**, 5HT2B (PDB code: 5TVN). **c**, DRD2. **d**, DRD3 (PDB code: 3PBL). **e**, DRD4 (PDB code: 5WIU). **f**, ACM1 (PDB code: 5CXV). **g**, ACM2 (PDB code: 3UON). **h**, ACM3 (PDB code: 4ADJ). **i**, ACM4 (PDB code: 4DSG). **j**, HRH1 (PDB code: 3RZE). **k**, ADRB1 (PDB code: 2VT4). **l**, ADRB2 (PDB code: 2RH1). **m**, DRD2. **n**, Conserved EL2 hydrophobic residues (red box) are located two residues away from a conserved cysteine that forms a disulphide bridge between EL2 and TMIII. Notable exceptions to the presence of a hydrophobic residue are DRD1 and DRD5, which contain a serine, and HRH1 and HRH4, which contain a threonine and proline, respectively.

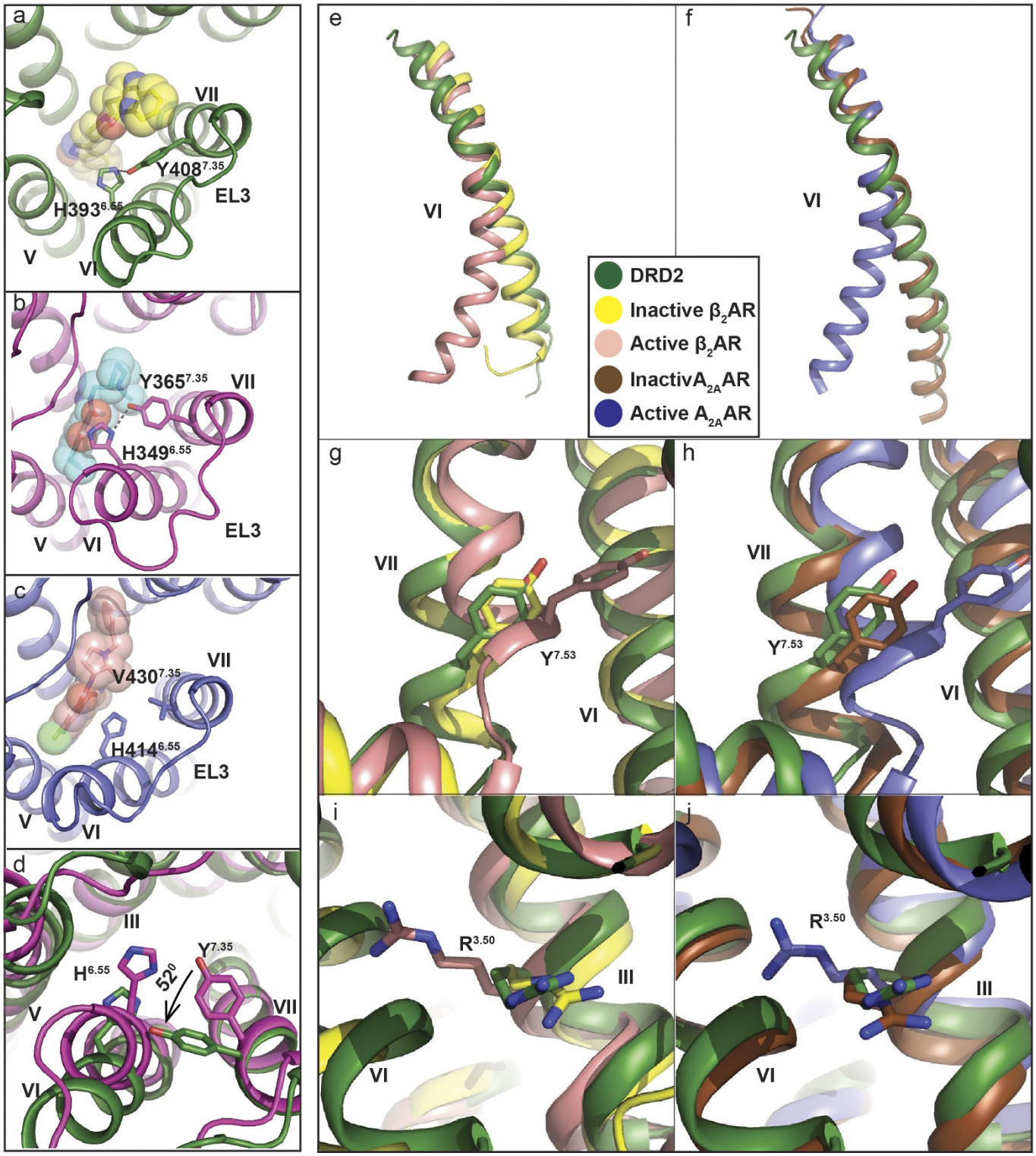

Extended Data Figure 3 | Comparison of D2 receptors viewed from the extracellular side, and structural alignment with β2AR and A2AR reveals an inactive state of DRD2. a–d, DRD2, green; DRD3, magenta (PDB code: 3PBL); DRD4, blue (PDB code: 5WIU). Risperidone (yellow), eticlopride (cyan) and nemonapride (light pink) are shown as sticks and spheres. Displacements of $H^{6.55}$ and $Y/V^{7.35}$ are shown at DRD2 (**a**), DRD3 (**b**) and DRD4 (**c**). **d**, Views from the extracellular side of DRD2 and DRD3. **e**, **f**, Superposition of TMVI at DRD2 (green), inactive β2AR (yellow, PDB code: 2RH1), active β2AR (light pink, PDB code: 3SN6), inactive A2AR (brown, PDB code: 3REY) and active A2AR (blue, PDB code: 5G53) aligned through helices I–IV. **g–j**, Cytoplasmic view of alignment between DRD2 and active and inactive β2AR (**g**, **h**) or A2AR (**i**, **j**). Rearrangements of two highly conserved residues ($Y^{7.53}$ and $R^{3.50}$) within the core of the receptor are shown as sticks. Ligands are omitted for clarity and hydrogen bonds are shown as grey dotted lines.

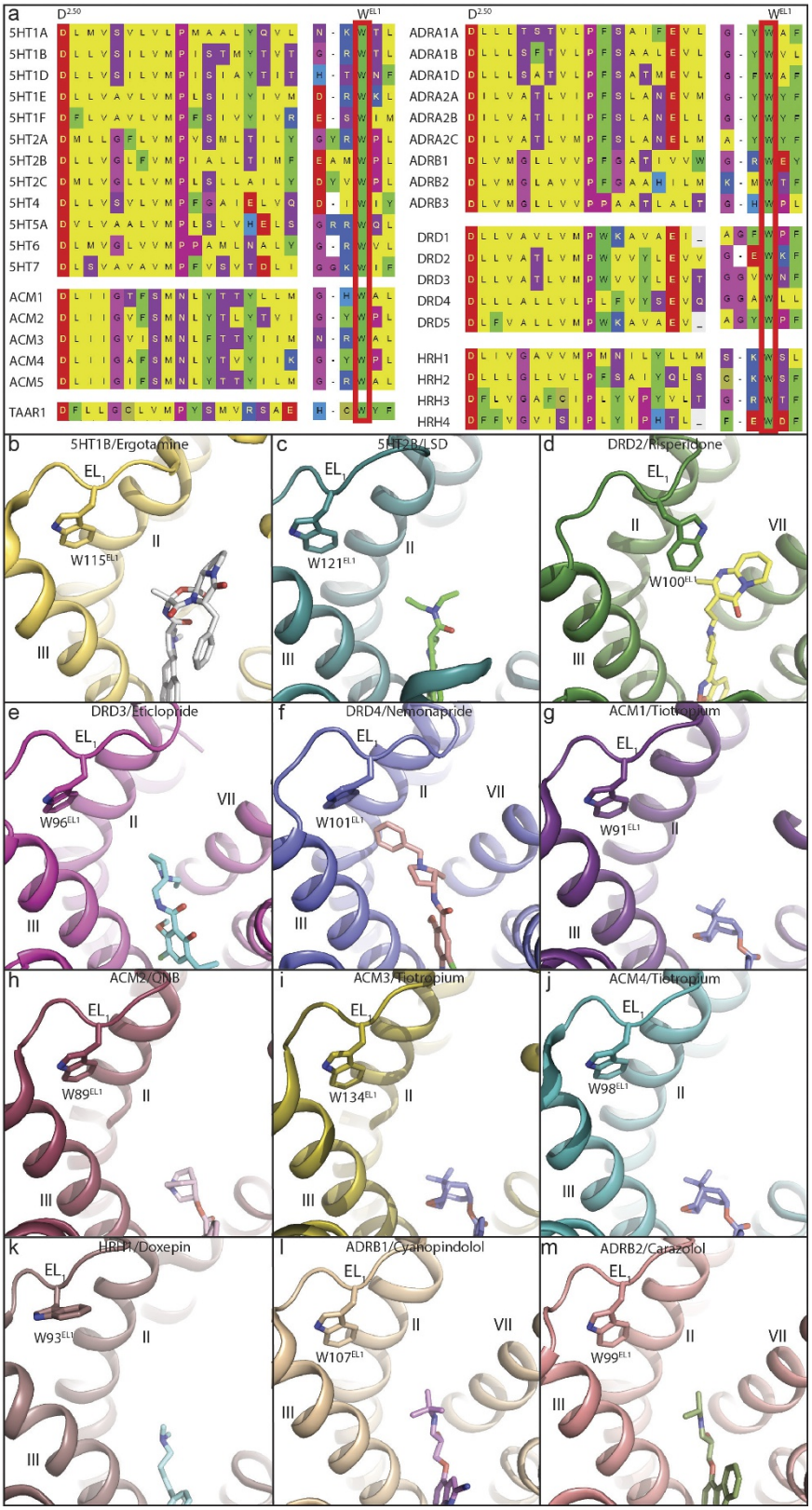

Extended Data Figure 4 | Conserved Trp of EL1 in all available aminergic receptor structures shows its unique position in DRD2–risperidone. Receptors are shown as cartoons. Ligands and residues are shown as sticks. **a**, Conserved Trp residues of EL1 are shown in red boxes. **b**, 5HT1B (PDB code: 4IAR). **c**, 5HT2B (PDB code: 5TVN). **d**, DRD2. **e**, DRD3 (PDB code: 3PBL). **f**, DRD4 (PDB code: 5WIU). **g**, ACM1 (PDB code: 5CXV). **h**, ACM2 (PDB code: 3UON). **i**, ACM3 (PDB code: 4ADJ). **j**, ACM4 (PDB code: 4DSG). **k**, HRH1 (PDB code: 3RZE). **l**, ADRB1 (PDB code: 2VT4). **m**, ADRB2 (PDB code: 2RH1).

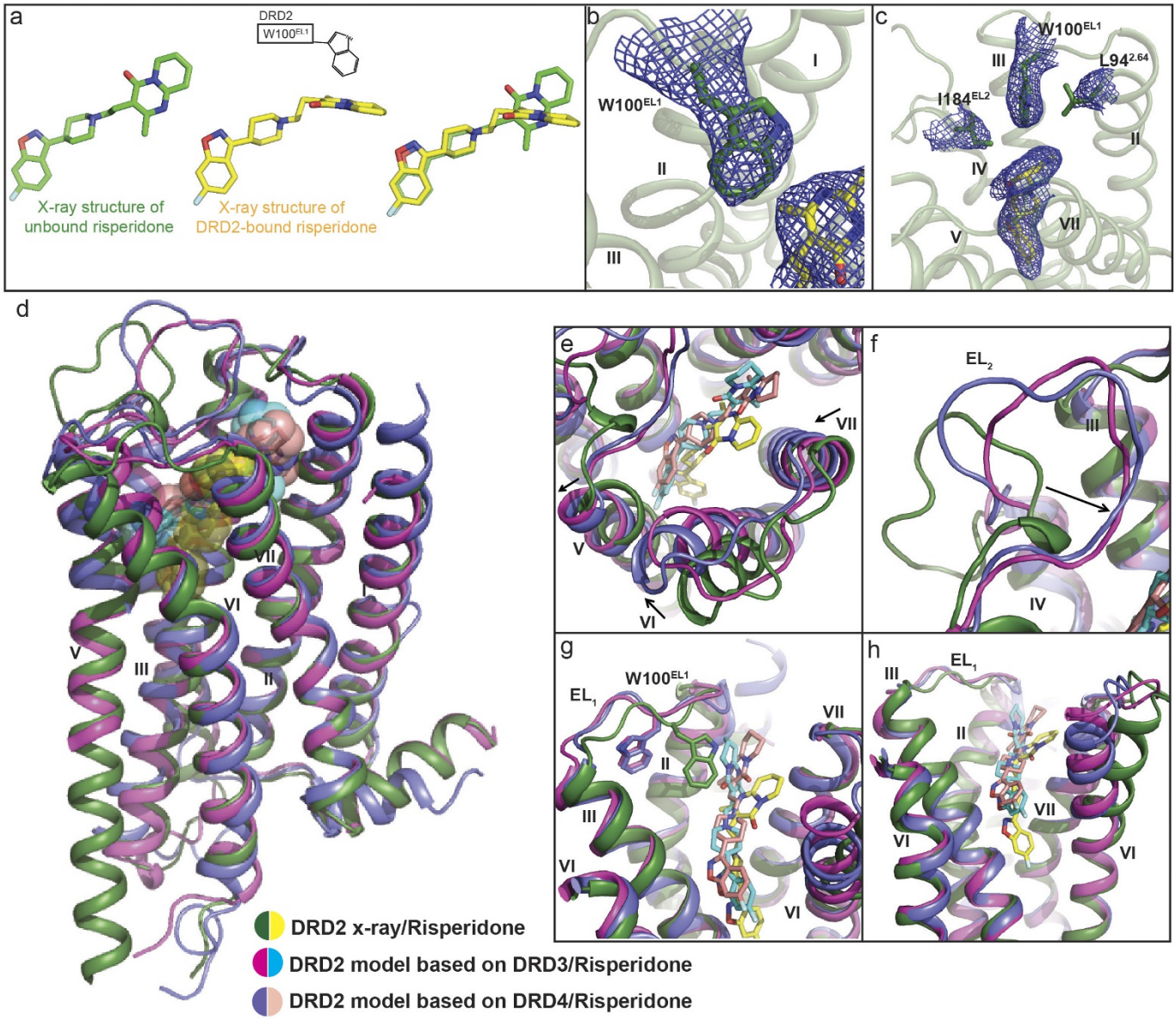

Extended Data Figure 5 | Risperidone has distinct poses in solution and in complex with DRD2, and comparison of X-ray structure and model of DRD2. a, Trp100^{EL1} determines the configuration of the tetrahydropyridopyrimidinone moiety of risperidone. Structure of unbound risperidone shown in green and DRD2-bound risperidone shown in yellow. **b**, Electron density ($2F_o$–F_c maps, blue mesh) for W100^{EL1} in the DRD2–risperidone complex (contoured at 1.0σ). **c**, $2F_o$–F_c electron density map (blue mesh) of Leu94$^{2.64}$, Trp100^{EL1}, Ile184^{EL2} and risperidone (yellow) contoured at 0.8σ. **d**, Overall view of DRD2–risperidone X-ray structure and model. **e**–**h**, Comparison of X-ray structure and model of DRD2. In **d**–**h**, DRD2 X-ray structure and model are shown as cartoons, with the X-ray structure in green and the model in magenta or blue. Risperidone is shown in the X-ray structure as yellow spheres or sticks, and in the model as cyan or light pink.

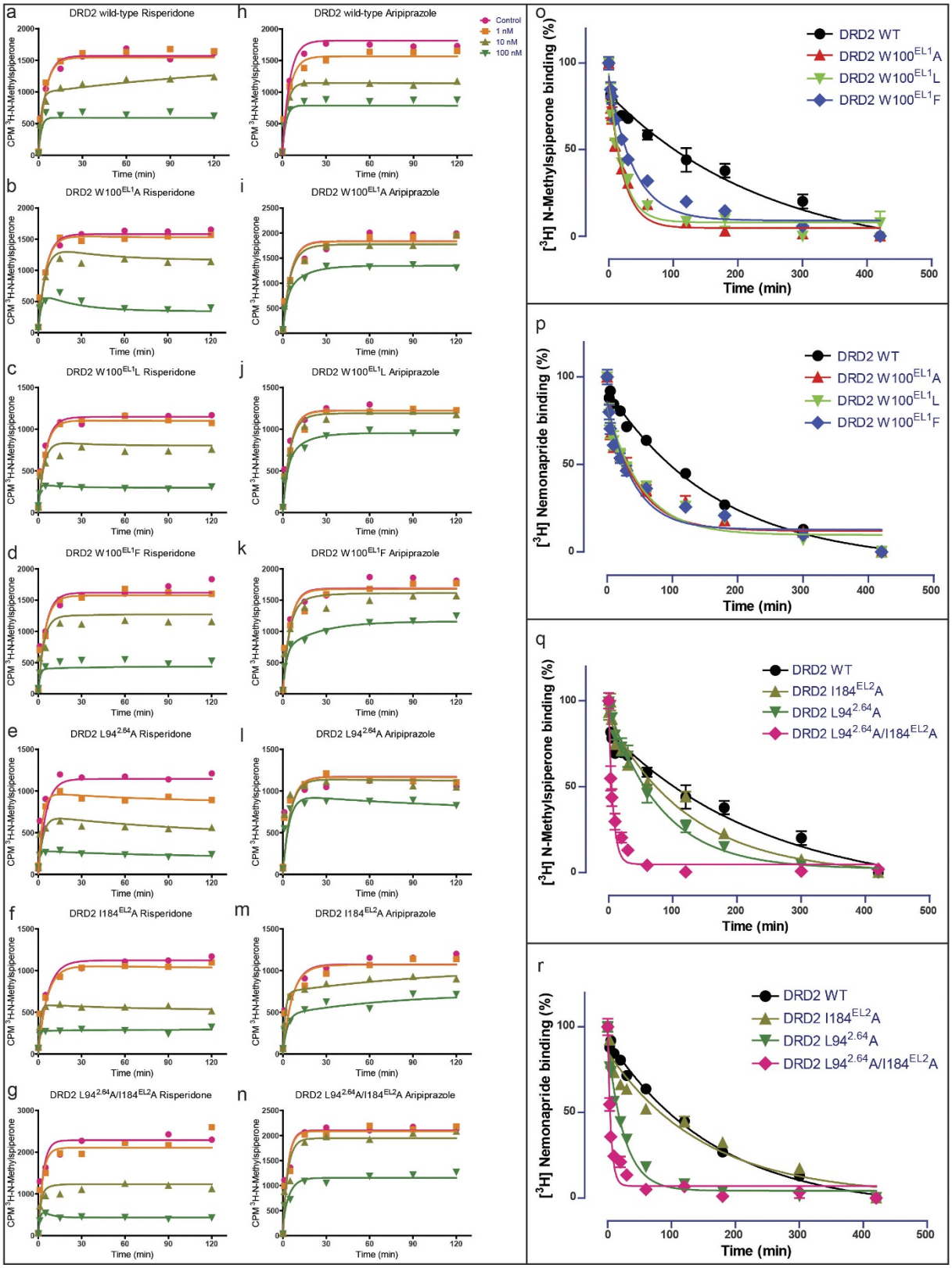

Extended Data Figure 6 | Patch residues of the DRD2 orthosteric pocket impair the dissociation rates of risperidone, aripiprazole, *N*-methylspiperone and nemonapride. **a**–**g**, Comparison of risperidone dissociation from wild-type DRD2 (**a**) and W100^{EL1}A (**b**), W100^{EL1}L (**c**), W100^{EL1}F (**d**), L94$^{2.64}$A (**e**), I184^{EL2}A (**f**) or L94$^{2.64}$A/I184^{EL2}A (**g**) mutants. **h**–**n**, Comparison of aripiprazole dissociation from wild-type DRD2 (**h**) and W100^{EL1}A (**i**), W100^{EL1}L (**j**), W100^{EL1}F (**k**), L94$^{2.64}$A (**l**), I184^{EL2}A (**m**) or L94$^{2.64}$A/I184^{EL2}A (**n**) mutants. **o**, **p**, Comparison of *N*-methylspiperone (**o**) or nemonapride (**p**) dissociation from wild-type DRD2 and W100^{EL1}A, W100^{EL1}L or W100^{EL1}F mutants ($n = 3$). **q**, **r**, Comparison of *N*-methylspiperone (**q**) or nemonapride (**r**) dissociation from wild-type DRD2 and L94$^{2.64}$A, I184^{EL2}A or L94$^{2.64}$A/I184^{EL2}A mutants. All data are mean ± s.e.m. of four independent assays ($n = 4$ independent experiments). Error bars in **o**–**r** denote s.e.m. from four independent assays.

Extended Data Table 1 | Affinities of antipsychotic drugs for thermostabilized mutant and wild-type DRD2

Receptor K_i, nM ($pK_i \pm$ SEM)	Risperidone	Aripiprazole	N-Methylspiperone	Nemonapride	Bifeprunox
DRD2 wild-type	1.91 (8.84±0.19)	6.28 (8.21±0.05)	0.04 (11.06±0.18)	0.03 (11.06±0.10)	1.04 (9.52±0.38)
DRD2 I122$^{3.40}$A / L375$^{6.37}$A / L379$^{6.41}$A	1.86 (9.10±0.38)	1.25 (8.91±0.04)	0.09 (11.01±0.11)	0.05 (11.03±0.06)	0.24 (9.62±0.02)
DRD2-T4L (Sf9) I122$^{3.40}$A / L375$^{6.37}$A / L379$^{6.41}$A	3.13 (8.57±0.18)	1.88 (8.73±0.02)	0.06 (11.02±0.04)	0.09 (11.03±0.33)	0.57 (9.25±0.03)

Data represent mean K_i ($pK_i \pm$ s.e.m.) for competition-binding experiments using [^{3}H]-*N*-methylspiperone (0.8–1.0 nM) as radioligand. All data are the mean ± s.e.m of three independent assays ($n = 3$ independent experiments).

Extended Data Table 2 | Data collection and refinement statistics

Structure	Human DRD2 (ΔN/ΔICL3$_{T4L}$/ΔC)-Risperidone complex
Data Collection	APS, GMCA/CAT 23ID-B/D, 10 µm microfocus beam
Crystals	20
Resolution range	30.00 - 2.90 (2.99 - 2.90)
Space group	$P2_12_12_1$
Unit cell Dimensions a, b, c (Å)	50.98 72.52 151.31
Unique reflections	12826 (889)
Multiplicity	5.5 (2.5)
Completeness (%)	97.3 (86.9)
Mean I/σ(I)	15.2 (1.0)
R_{merge} (%)	13.4 (73.8)
$CC_{1/2}$ (%)	99.4 (53.5)
Refinement Statistics	
Reflections used in refinement	12826 (889)
Reflections used for R-free	622 (40)
R-work (%)	22.6 (37.4)
R-free (%)	24.9 (34.1)
Number of Atoms	
DRD2	1948
T4L	1176
Risperidone	30
Lipid and other	82
Overall B-factors (Å^2)	
Receptor	84.1
T4L	97
Risperidone	75.8
Lipids, water, other	86.8
Model Statistics	
RMSD-bonds (Å)	0.004
RMSD-angles (°)	0.56
Ramachandran favored (%)#	97.36
Ramachandran allowed (%)#	2.64
Ramachandran outliers (%)#	0.00
Rotamer outliers (%)#	0.67
Clashscore#	3.99

Highest resolution shell is shown in parentheses.
*$R_{merge} = \Sigma hkl\ |I(hkl) - <I(hkl)>| / \Sigma hkl\ (hkl)$, where $<I(hkl)>$ is the mean of the symmetry equivalent reflections of $I(hkl)$.
#As defined in MolProbity.

Extended Data Table 3 | Affinity of risperidone and nemonapride for ligand-binding-pocket mutants of the D_2 dopamine receptor

Receptor	Risperidone		Nemonapride	
	K_i, nM ($pK_i \pm$ SEM)	ΔpK_i (mutant-WT)	K_d, nM ($pK_d \pm$ SEM)	ΔpK_d (mutant-WT)
DRD2 wild-type	4.50 (8.41 ± 0.07)	--	0.21 (9.69 ± 0.06)	--
DRD2 $W100^{EL1}A$	8.14 (8.19 ± 0.13)	-0.21	1.97 (8.71 ± 0.02)	-0.98
DRD2 $F110^{3.28}A$	36.89 (7.48 ± 0.09)	-0.93	0.17 (9.77 ± 0.03)	0.08
DRD2 $D114^{3.32}A$	>10000	--	8.10 (8.09 ± 0.04)	-1.60
DRD2 $V115^{3.33}A$	3.07 (8.52 ± 0.04)	0.11	0.84 (9.08 ± 0.02)	-0.61
DRD2 $C118^{3.36}A$	4.84 (8.32 ± 0.01)	-0.09	0.40 (9.40 ± 0.02)	-0.29
DRD2 $T119^{3.37}A$	177.19 (6.83 ± 0.12)	-1.58	0.43 (9.38 ± 0.06)	-0.31
DRD2 $I122^{3.40}A$	13.87 (7.97 ± 0.13)	-0.44	0.30 (9.52 ± 0.01)	-0.17
DRD2 $S197^{5.46}A$	1.22 (8.92 ± 0.03)	0.51	0.43 (9.37 ± 0.01)	-0.32
DRD2 $F198^{5.47}A$	41.95 (7.38 ± 0.03)	-1.02	0.76 (9.12 ± 0.02)	-0.57
DRD2 $F382^{6.44}A$	57.70 (7.25 ± 0.05)	-1.16	0.30 (9.53 ± 0.05)	-0.16
DRD2 $W386^{6.48}A$	>10000	--	4.02 (8.40 ± 0.04)	-1.29
DRD2 $F389^{6.51}A$	2992 (5.65 ± 0.17)	-2.76	4.70 (8.35 ± 0.08)	-1.34
DRD2 $F390^{6.52}A$	31.20 (7.61 ± 0.15)	-0.80	1.30 (8.89 ± 0.03)	-0.80
DRD2 $Y408^{7.35}A$	13.63 (7.95 ± 0.13)	-0.46	0.18 (9.76 ± 0.02)	0.07
DRD2 $T412^{7.39}A$	102.68 (7.02 ± 0.08)	-1.77	4.92 (8.33 ± 0.10)	-1.36
DRD2 $Y416^{7.43}A$	2772 (5.61 ± 0.15)	-2.80	0.88 (9.06 ± 0.01)	-0.63

Data represent mean K_i ($pK_i \pm$ s.e.m.) for competition-binding experiments and K_d ($pK_d \pm$ s.e.m.) for homologous competition-binding experiments using [^{3}H]-nemonapride (0.1–0.5 nM) as radioligand. All data are mean ± s.e.m of three independent assays ($n = 3$ independent experiments).

Extended Data Table 4 | Compound dissociation and association rates on wild-type and mutant DRD2

Compound	Receptor	Residence Time, min (k_{off} ± SEM) min^{-1}	k_{on} ± SEM, M^{-1} min^{-1}	K_d, nM (pK_d ± SEM)
Aripiprazole	DRD2 wild-type	154 (0.0065 ± 0.0004)	7.68×10^5 ± 4.94×10^5	9.43 (8.03 ± 0.07)
	DRD2 W100^{EL1}A	15 (0.067 ± 0.015) *p=0.006	2.48×10^5 ± 6.5×10^4	273 (6.56 ± 0.02)
	DRD2 W100^{EL1}L	14 (0.071 ± 0.0007) *p=0.006	1.89×10^5 ± 3.7×10^4	387 (6.42 ± 0.08)
	DRD2 W100^{EL1}F	26 (0.038 ± 0.007) *p=0.008	6.32×10^5 ± 8.5×10^4	62.8 (7.22 ± 0.14)
	DRD2 L94$^{2.64}$A	59 (0.017 ± 0.002) n.s.	1.23×10^6 ± 1.06×10^6	49.8 (7.56 ± 0.52)
	DRD2 I184^{EL2}A	100 (0.010 ± 0.001) n.s.	6.65×10^5 ± 5.1×10^4	15.5 (7.81 ± 0.03)
	DRD2 L94$^{2.64}$A/I184^{EL2}A	3 (0.32 ± 0.06) *p=0.005	2.93×10^6 ± 2.58×10^6	413 (6.64 ± 0.52)
N-Methylspiperone	DRD2 wild-type	250 (0.004 ± 0.0003)	2.34×10^8 ± 6×10^7	0.018 (10.75 ± 0.08)
	DRD2 W100^{EL1}A	21 (0.048 ± 0.0079) *p=0.0073	1.65×10^8 ± 6×10^7	0.31 (9.51 ± 0.08)
	DRD2 W100^{EL1}L	20 (0.050 ± 0.0064) *p=0.0072	1.72×10^8 ± 4×10^7	0.29 (9.53 ± 0.03)
	DRD2 W100^{EL1}F	38 (0.026 ± 0.00003) *p=0.0083	2.08×10^8 ± 5×10^7	0.13 (9.89 ± 0.10)
	DRD2 L94$^{2.64}$A	77 (0.013 ± 0.0047) n.s.	2.08×10^8 ± 4×10^7	0.062 (10.21 ± 0.08)
	DRD2 I184^{EL2}A	128 (0.0078 ± 0.00004) n.s.	1.70×10^8 ± 3×10^7	0.048 (10.33 ± 0.08)
	DRD2 L94$^{2.64}$A/I184^{EL2}A	6 (0.170 ± 0.063) *p=0.0064	1.62×10^8 ± 1×10^7	1.02 (9.01 ± 0.14)
Nemonapride	DRD2 wild-type	167 (0.006 ± 0.0002)	2.0×10^8 ± 5×10^7	0.031 (10.52 ± 0.09)
	DRD2 W100^{EL1}A	43 (0.023 ± 0.001) *p=0.002	1.17×10^8 ± 2×10^7	0.19 (9.75 ± 0.14)
	DRD2 W100^{EL1}L	45 (0.022 ± 0.0018) *p=0.003	1.07×10^8 ± 3×10^7	0.20 (9.70 ± 0.02)
	DRD2 W100^{EL1}F	40 (0.025 ± 0.0019) *p=0.002	2.03×10^8 ± 6×10^7	0.13 (9.90 ± 0.10)
	DRD2 L94$^{2.64}$A	26 (0.039 ± 0.0033) *p=0.0015	2.97×10^8 ± 5×10^7	0.13 (9.88 ± 0.03)
	DRD2 I184^{EL2}A	149 (0.0067 ± 0.0004) n.s.	9.60×10^7 ± 7×10^6	0.07 (10.16 ± 0.06)
	DRD2 L94$^{2.64}$A/I184^{EL2}A	5 (0.20 ± 0.0048) *p=0.0009	2.89×10^8 ± 1×10^8	0.82 (9.12 ± 0.19)

Data were acquired by association and dissociation kinetic experiments conducted in parallel at room temperature using [^{3}H]-*N*-methylspiperone (0.8–1.0 nM) for aripiprazole and *N*-methylspiperone or [^{3}H]-nemonapride (0.8–1.0 nM) for nemonapride. Estimates of k_{off}, k_{on}, and K_d were obtained from four independent experiments. Residence time was calculated as $1/k_{off}$. All data are mean ± s.e.m. of four independent assays ($n = 4$ independent experiments). *statistically significant differences between wild-type and mutant receptors; n.s., not significant; *P* values are indicated, unpaired two-tailed Student's *t*-test.